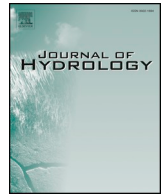




ELSEVIER

Contents lists available at ScienceDirect

Journal of Hydrology

journal homepage: www.elsevier.com/locate/jhydrol

Research papers

Hydrologic model parameterization using dynamic Landsat-based vegetative estimates within a semiarid grassland



Mark A. Kautz^{a,b,*}, Chandra D. Holifield Collins^b, D. Phillip Guertin^a, David C. Goodrich^b, Willem J. van Leeuwen^a, C. Jason Williams^b

^a University of Arizona, 1230 E. Speedway Boulevard, P.O. Box 210104, Tucson, AZ 85721, USA

^b USDA ARS Southwest Watershed Research Center, 2000 E. Allen Road, Tucson, AZ 85719, USA

ARTICLE INFO

This manuscript was handled by Emmanouil Anagnostou

Keywords:

Rangeland Hydrology and Erosion Model
KINEROS
Landsat
Remote sensing
Surface runoff
Ecohydrology

ABSTRACT

The use of hydrologic models to assess long-term watershed condition through repeated simulations of runoff and erosion is one common approach for rangeland health evaluation. However, obtaining vegetative data of appropriate spatiotemporal resolution for model parameterization can be difficult. The goal of this research was to assess the utility of using time-varying, Landsat-derived vegetative values to parameterize an event-based, watershed-scale hydrologic model. This study was conducted on a small, instrumented grassland watershed in the USDA Agricultural Research Service operated Walnut Gulch Experimental Watershed in southeastern, Arizona. Cloud-free Landsat scenes were acquired over the watershed for the years 1996–2014. The Soil Adjusted Total Vegetation Index (SATVI) was calculated for each image and calibrated using ground measured data to produce a time series of satellite-based foliar cover rasters. These values were used to parameterize the Rangeland Hydrology and Erosion Model (RHEM) for 26 rainfall-runoff events with corresponding observed data. Three parameterization scenarios using these data aggregated to different temporal resolutions (static, long-term mean, annual mean, and intra-annual values) were compared to a static literature-based scenario for evaluation. The linear relationship between field-measured foliar cover and SATVI showed statistically significant agreement with $R^2 = 0.85$ and $p < 0.05$. Simulated runoff volume and peak flow rate using the three remotely sensed parameterization scenarios improved upon that of the literature-based scenario, with the annual mean scenario performing the best of the three temporal aggregations. The methodological framework outlined here provides a means for improved parameterization for watershed-scale modelling where vegetative data may be scarce or unobtainable for long-term analysis.

1. Introduction

The acceleration of rangeland degradation has emerged as a major environmental concern in recent decades (MEA, 2005; Reynolds et al., 2007; Schlesinger et al., 1990). It is estimated that 10–20% of global rangelands have been severely degraded, reducing the capacity to provide many valuable ecosystem services including agricultural and livestock production, carbon sequestration, and biodiversity (Asner et al., 2004; Havstad et al., 2007). Rangelands are generally limited by water and soil nutrients, and exhibit great spatial and temporal variability in productivity (Havstad et al., 2007). Vegetative condition in these regions can vary greatly with time, as vegetation is easily diminished and the recovery time can take decades (Pilgrim et al., 1988).

Strong relationships between ecological and hydrological processes exist in these semiarid environments (Ludwig et al., 2005). Shifts in

vegetative composition and productivity from natural and anthropogenic pressures include: woody species encroachment on native grasslands (Asner et al., 2003; Scholes and Archer, 1997); increases in invasive grasses (DiTomaso, 2000; Polyakov et al., 2010); drought induced vegetative die-off (Breshears et al., 2005; Moran et al., 2014); and mortality from land mismanagement (Greene et al., 1994; McIvor et al., 1995). These changes in vegetation can ultimately lead to increased surface runoff and soil erosion through: reduced infiltration rates (Dadkhah and Gifford, 1980; Dunne et al., 1991); decreased surface roughness (Cerdà, 1997; Ludwig et al., 2005; Weltz et al., 1992); decreased canopy interception (Burgy and Pomeroy, 1958; Thurow et al., 1987); and degraded aggregate stability of the soil (Barthès and Roose, 2002; Cantón et al., 2009; Holifield Collins et al., 2015).

Plot-scale studies have played an important role in gaining understanding of hydrologic processes within these environments. It has been

* Corresponding author at: USDA ARS Southwest Watershed Research Center, 2000 E. Allen Road, Tucson, AZ 85719, USA.

E-mail address: mark.kautz@ars.usda.gov (M.A. Kautz).

<https://doi.org/10.1016/j.jhydrol.2019.05.044>

Received 14 November 2018; Received in revised form 5 May 2019; Accepted 13 May 2019

Available online 15 May 2019

0022-1694/ Published by Elsevier B.V.

widely reported that as vegetative cover decreases, surface runoff and erosion rates increase within a rangeland environment (Nearing et al., 2005; Puigdefábregas, 2005; Rogers and Schumm, 1991; Zuazo et al., 2008). There is general agreement that a threshold of 30–50% grass cover is needed to significantly deter runoff and soil erosion in semiarid environments (Gutierrez and Hernandez, 1996; Holifield Collins et al., 2015; Pan and Shanguan, 2006).

While plot-scale experiments offer a great deal of control, they lack representation of the complexities of the natural system in which they exist. There is a growing need for information on the large-scale ecohydrological effects of climate induced alterations of vegetation and precipitation regimes (Newman et al., 2006; Seyfried and Wilcox, 1995). Scaling up in size from plot studies to catchment size studies introduces a more realistic representation of the ecological system, with the heterogeneities in vegetation, topography, soil and climate represented. However, the large spatial extent and spatiotemporal heterogeneity of these regions have made monitoring and quantitatively assessing the large-scale effects of these ecohydrological landscape changes a challenge.

Hydrologic models are one practical tool for quantifying runoff and erosion rates in rangelands (Hernandez et al., 2013; Nearing et al., 2011). Modelling allows for relationships and processes observed at small scales to be extrapolated spatially and temporally to a larger scale, enabling studies that may not be physically or economically feasible by traditional field methods (Nearing et al., 1989; Wainwright et al., 2000). The ability to predict runoff and erosion using measurable biophysical model inputs provides land managers with scientifically-based information for land management decisions. The Rangeland Hydrology and Erosion Model (RHEM) was developed specifically for hillslope-scale use in rangeland environments, adapting the central algorithms from the Water Erosion Prediction Project (WEPP) model to the unique hydrologic characteristics of these semiarid regions (Hernandez et al., 2017; Nearing et al., 2011). Parameter estimation equations in RHEM utilize physically quantifiable inputs including soil texture, slope characteristics, vegetation cover, and ground cover (Al-Hamdan et al., 2013; Al-Hamdan et al., 2017; Hernandez et al., 2017). These commonly measured inputs allow for intuitive simulation of vegetation or ground cover changes due to management or disturbance (Hernandez et al., 2013; Nouwakpo et al., 2016a; Williams et al., 2016a). Watershed-scale modelling with RHEM can be achieved by routing hillslope simulations through a network of channels using the KINEROS2 (K2) model within the Automated Geospatial Watershed Assessment Tool (AGWA) geospatial environment (Ross, 2013).

The use of models in long-term, watershed-scale hydrological monitoring is limited by the availability of corresponding vegetative data of sufficient spatiotemporal resolution for input. While localized transect-based vegetation measurements are appropriate for modelling at the hillslope scale, these measurements are often prohibitive at the watershed scale due to time and cost constraints. Furthermore, the existence of such data with historic or replicated measurements for long-term monitoring or comparison purposes is sparse. These data limitations are a key obstacle for large-scale hydrologic modelling in arid and semiarid regions (Goodrich et al., 2012; Pilgrim et al., 1988; Seyfried and Wilcox, 1995).

A common approach for watershed-scale model parameterization is to associate literature-based parameter values with land cover classes based on national land cover geospatial data sets, e.g., the National Land Cover Database (NLCD) and the North American Lands Change Monitoring System (NALCMS) (Goodrich et al., 2012; Hernandez et al., 2000; Miller et al., 2002; Niraula et al., 2012; Norman et al., 2010). Deriving detailed vegetative parameters from these sources can be problematic, as land cover classes are often generalized across many plant communities and can cover large areas.

The use of satellite-based remote sensing on rangelands has been shown effective for quantifying vegetative parameters including biomass, leaf area index, and foliar cover (Booth and Tueller, 2003; Hunt

et al., 2003; Qi et al., 2002; Wallace et al., 2006). The Landsat earth-observing satellites are particularly appropriate for ecological monitoring and vegetation change detection at the regional or watershed scale (Vogelmann et al., 2012). These data offer the necessary spatiotemporal and spectral resolution for characterizing vegetation typical of rangelands and capturing both long-term trends and intra-annual variability across large regions (Huete, 1988; Marsett et al., 2006; Purevdorj et al., 1998; Xie et al., 2008). The release of a free Landsat archive (1984-present) to the public provides a cost effective, easily obtainable resource for long-term vegetation monitoring (Markham and Helder, 2012; Masek et al., 2006; Wulder et al., 2012). Recent studies using Landsat data have shown advancements in identifying degraded grasslands (Fassnacht et al., 2015); improved change detection of grasslands (Tarantino et al., 2016); detection of grazing effects and management practices in grasslands (Guo et al., 2015; Xu et al., 2018; Sibanda et al., 2016); and identifying plant communities in rangelands (Villarreal et al., 2016).

The incorporation of remotely sensed data into spatially distributed hydrological models provides a means for model parameterization at large spatial scales and with improved temporal frequency. Spatially distributed, watershed-scale, vegetative model inputs allow for a more realistic representation of the distribution and structure of vegetation that govern rangeland hydrology (Cadaret et al., 2016; Nouwakpo et al., 2016b; Puigdefábregas, 2005; Williams et al., 2016a). Additionally, long-term, dynamic vegetative data records facilitate analyses of hydrologic response to landscape change and disturbance such as fire, grazing and plant community alterations (Ebel and Martin, 2017; Flerchinger et al., 2016; Park et al., 2017; Spaeth et al., 2016; Williams et al., 2016b). However, uncertainty remains in how large-scale spatial and temporal variability may affect model results (Seyfried and Wilcox, 1995; Reynolds et al., 2017; Urban, 2005). The goal of this research was to evaluate whether the inclusion of time-varying, Landsat-based foliar cover estimates improves runoff prediction within a RHEM/K2 modelling framework. Thus, the specific objectives of the study were to: 1) quantify watershed-scale vegetation and ground cover for model parameterization and calibration of a remotely-sensed foliar cover dataset; 2) develop a 20-year time series of field-calibrated, Landsat-based foliar cover for the study area; and 3) evaluate model performance for a default literature-based parameterization approach versus three parameterization scenarios incorporating the remotely sensed vegetative estimates of varying temporal aggregation.

2. Methods

2.1. Site description

This research was conducted on the Kendall grassland located within the USDA Agricultural Research Service (ARS) Walnut Gulch Experimental Watershed (WGEW) in southeastern Arizona (Fig. 1). The climate of the region is semiarid, with a mean annual temperature of 18 °C and mean annual precipitation of 315 mm (1961–2015) across the WGEW. Approximately 65% of the annual precipitation occurs between July and September during the North American Monsoon. Monsoon precipitation is dominated by high-intensity, spatially localized, convective thunderstorms from which large amounts of runoff and flash flooding can occur. Winter precipitation is dominated by large-scale, low-intensity frontal storms that generally do not produce surface runoff in the WGEW.

The Kendall subwatershed is located in the upper portion of the WGEW (31.74°N, 109.94°W). The watershed has a drainage area of 0.02 km² and average slope gradient of 12.3%. The soils are an Elgin (50%)-Stronghold (40%) complex with a fine, gravelly sandy loam upper horizon and clay components below 2.5 cm (Breckenfeld et al., 1995). The watershed drains into a densely vegetated swale near the outlet of the watershed through concentrated flow paths. The swale serves as a deposition zone at which increased infiltration and sediment

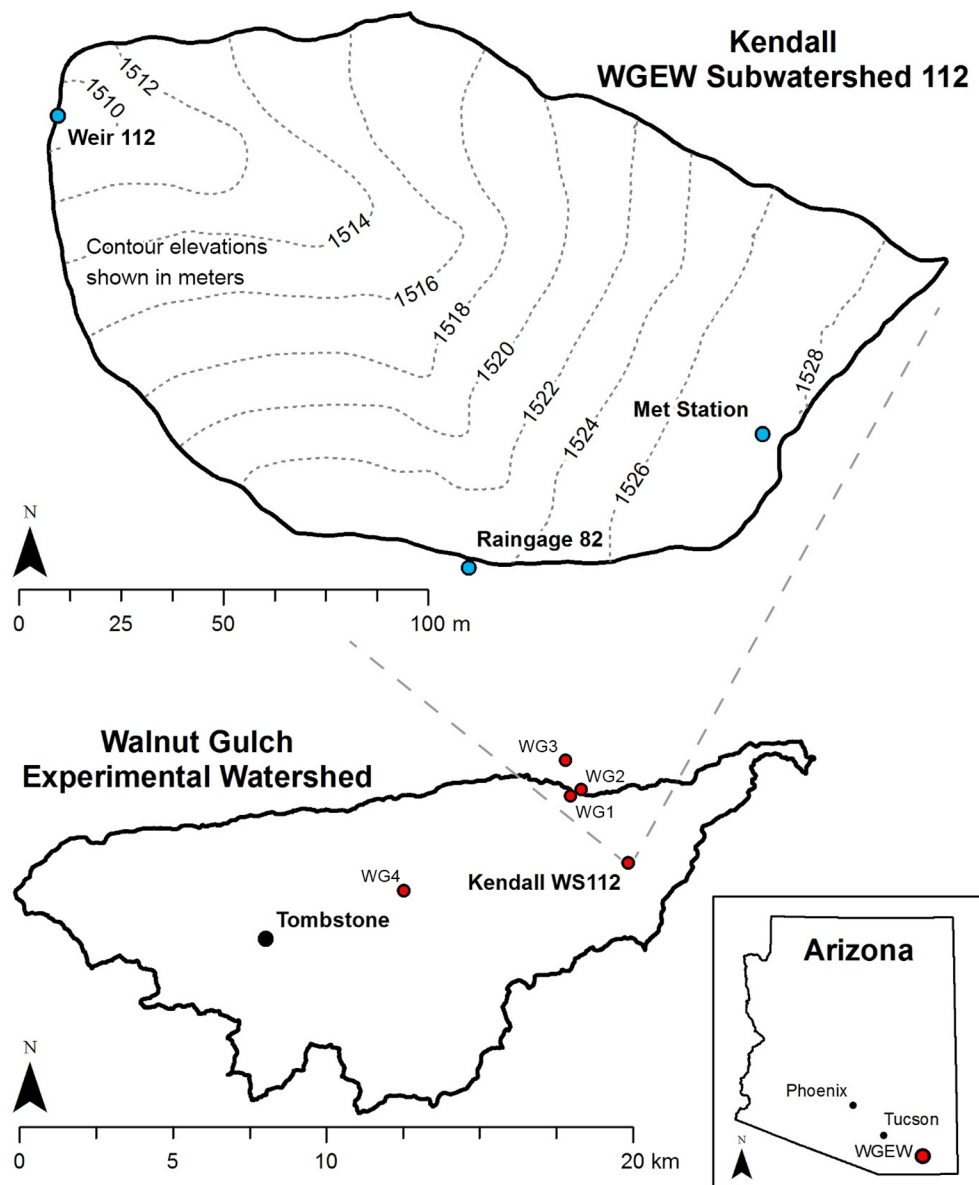


Fig. 1. The Kendall watershed study site and sparse cover calibration locations at Walnut Gulch Experimental Watershed (WGEW) with watershed boundary and detail with topography and instrumentation.

storage occur (Nearing et al., 2005). Kendall is instrumented with a weighing type rain gauge, V-notch weir, pump sediment sampler, and meteorological station with Delta-T ThetaProbe soil moisture sensors at 5 and 15 cm depth (Goodrich et al., 2008; Keefer et al., 2008; Nichols et al., 2008; Stone et al., 2008a).

The vegetation of the watershed has historically been dominated by native bunchgrasses (Scott et al., 2010). Following an extended period of drought, many of the native grasses and shrubs died in 2006 and were replaced with forbs. Since then, the watershed has been dominated by the invasive bunchgrass *Eragrostis lehmanniana* (Lehmann lovegrass). The main period of vegetative productivity occurs from July–October in response to warm temperatures and monsoon precipitation. A short growth period for annual grasses and forbs may occur in early spring if winter precipitation is sufficient.

2.2. Methods workflow overview

The following sections describe the process in which a field-calibrated, remotely sensed foliar cover dataset was generated and

integrated into the hydrologic model for precipitation-runoff simulations (Fig. 2).

2.3. Landsat image acquisition

Multispectral imagery from Landsat 5 Thematic Mapper (TM) [1984–2012], Landsat 7 Enhanced Thematic Mapper Plus (ETM+) [1999–2015], and Landsat 8 Operational Land Imager (OLI) [2013–present] were used in this study. This series of satellites was designed to provide a continuous series of multispectral earth observations for global land surface monitoring at a spatial resolution of 30-m ground measured distance (Markham and Helder, 2012). The satellites have a repeat cycle of sixteen days, with each satellite in orbit offset by 8 days (e.g., TM and ETM+ or ETM+ and OLI). The definition of spectral bands varies slightly between satellites, but the data series can largely be considered continuous if atmospheric corrections are applied (Bryant et al., 2003, Roy et al., 2014). Surface reflectance data were used to minimize some of these differences and allow for time series analysis (Flood, 2014). No adjustments or calibration between satellites were

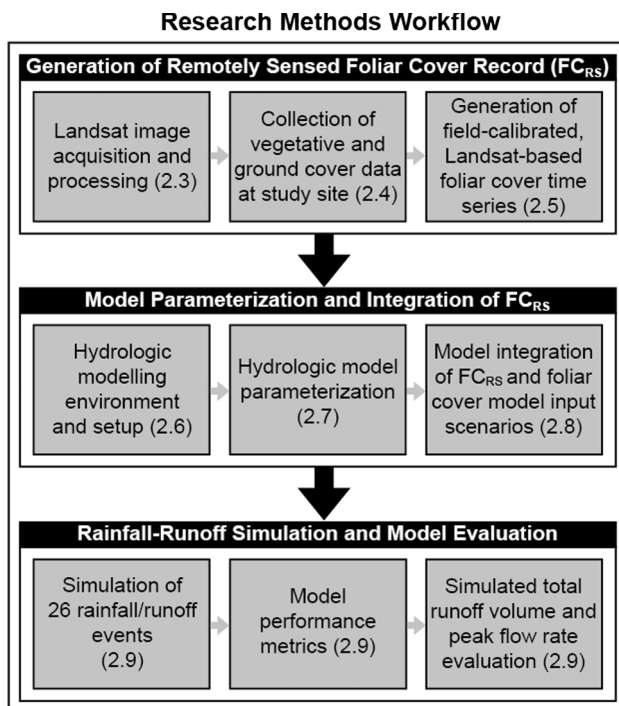


Fig. 2. Flowchart describing the methodological approach for integrating field calibrated, Landsat-based vegetative parameters into rainfall-runoff simulations.

performed and data obtained from the three satellites were considered to be a continuous data series in this study.

Cloud-free Landsat surface reflectance scenes (1996–2015) were acquired between April and December for World Reference System (WRS-2) Path: 36, Row: 38 through the United States Geological Survey (USGS) EarthExplorer (<http://earthexplorer.usgs.gov>) and Google Earth Engine (<http://earthengine.google.com>). TM and ETM+ surface reflectance products were processed using the Landsat Ecosystem Disturbance Adaptive Processing System (LEDAPS) method (Masek et al., 2006). The OLI surface reflectance product was calculated using the provisional Landsat Surface Reflectance Code [LaSRC] (Vermote et al., 2016). All ETM+ scenes were visually screened for the presence of scan line correction data gaps in the region immediately surrounding Kendall. The images were subsequently archived into a time series of surface reflectance scenes over the study domain.

2.4. Field data collection

Ten transects were established across Kendall to monitor vegetative and ground cover over the course of the 2015 growing season. Transects were arranged within 3 60 m × 60 m sampling blocks designed to register with four Landsat pixels (Fig. 3). Each sampling block contained three 80-m transects. The transects spanned the length of two Landsat pixels (60 m) with 10 m of extra length at each end to account for GPS error (transect locations were logged using a handheld GPS device with ± 5 m accuracy). Two-by-two-pixel sized blocks were chosen as the sampling area to compensate for uncertainty in registration during ground validation (Congalton, 1991, Stehman and Czaplewski, 1998).

Foliar cover and ground cover were measured at 0.5 m intervals along each transect using the line-point intercept method (Herrick et al., 2005). Canopy hits were classified by plant life-form as grass, shrub or forb as well as senescent or green. Ground cover hits were classified as bare soil, rock, litter or basal area by life-form (senescent or green).

Eight iterations of transect measurements were conducted between April 22, 2015 and October 28, 2015 on Kendall. Four additional transect locations (WG1-4) within WGEW were measured in grassland areas with sparse cover surrounding Kendall for use in Landsat calibration (Fig. 1). One transect block at each of these sites was measured between December 2, 2015 and December 7, 2015. The collection dates at all sites were designed to fall between Landsat 7 and Landsat 8 satellite overpasses to maximize the potential for acquiring a cloud-free satellite image with close proximity to ground measurements for calibration (Table 1).

2.5. Development of Landsat-based foliar cover

Three vegetation indices were calculated and evaluated for foliar cover estimation from the acquired Landsat surface reflectance scenes: the Normalized Difference Vegetation Index (NDVI), the Soil Adjusted Vegetation Index (SAVI), and the Soil Adjusted Total Vegetation Index (SATVI). NDVI is a commonly used vegetation index used for measuring green or photosynthetically active vegetation calculated as:

$$NDVI = \frac{\rho_{NIR} - \rho_{RED}}{\rho_{NIR} + \rho_{RED}}, \quad (1)$$

where ρ_{NIR} is surface reflectance in the near infrared band and ρ_{RED} is surface reflectance in the red band. This vegetation index functions under the premise that live green vegetation absorbs energy in the red wavelengths and reflects in the near infrared (NIR) lengths (Tucker, 1979). However, when used in areas with sparse vegetative cover soil reflectance from the underlying soil can inflate the index values erroneously (Huete, 1988). SAVI incorporates a soil adjustment factor (L) to account for this phenomenon and is calculated as:

$$SAVI = \frac{\rho_{NIR} - \rho_{RED}}{\rho_{NIR} + \rho_{RED} + L}(1 + L), \quad (2)$$

where ρ_{NIR} is surface reflectance in the near infrared band, ρ_{RED} is surface reflectance in the red band, and L is the soil adjustment factor. By varying the L factor between 0 (high vegetation density) and 1 (low vegetation density) the vegetation index can be calibrated to minimize the effect of background soil reflectance (Huete, 1988). An L factor of 0.5 was used here, representing moderate vegetative cover.

While NDVI and SAVI are measures of green vegetation, SATVI is a measure of both green and senescent vegetation (Marsset et al., 2006). SATVI is calculated as:

$$SATVI = \frac{\rho_{SWIR1} - \rho_{RED}}{\rho_{SWIR1} + \rho_{RED} + L}(1 + L) - \frac{\rho_{SWIR2}}{2} \quad (3)$$

where ρ_{SWIR1} is surface reflectance in the first shortwave infrared band, ρ_{SWIR2} is surface reflectance in the second shortwave infrared band, ρ_{RED} is surface reflectance in the red band, and L is the soil adjustment factor.

Linear regression analyses were performed between the total foliar cover (green and senescent) measured in the Kendall and WGEW blocks and the vegetation index images corresponding with the ground measurement dates (Table 1) to establish if any significant relationships existed (Hagen et al., 2012; Marsset et al., 2006). A spatial average of vegetation index values was calculated for the four Landsat pixels intersecting each study block for use in the regression analysis. The strength of correlation for each regression was evaluated using the coefficient of determination (R^2), Mean Absolute Error (MAE), and Root Mean Squared Error (RMSE). A time series of total foliar cover values (FC_{RS}), including green and senescent vegetation, was then produced by applying the best-performing vegetation index versus foliar cover relationship to the Landsat vegetation index data set.

In addition to foliar cover, basal and litter cover are required inputs for parameterizing the model. However, in this environment it is difficult to discern these values using downward-looking remotely sensed data. Therefore, allometric relationships were developed from the

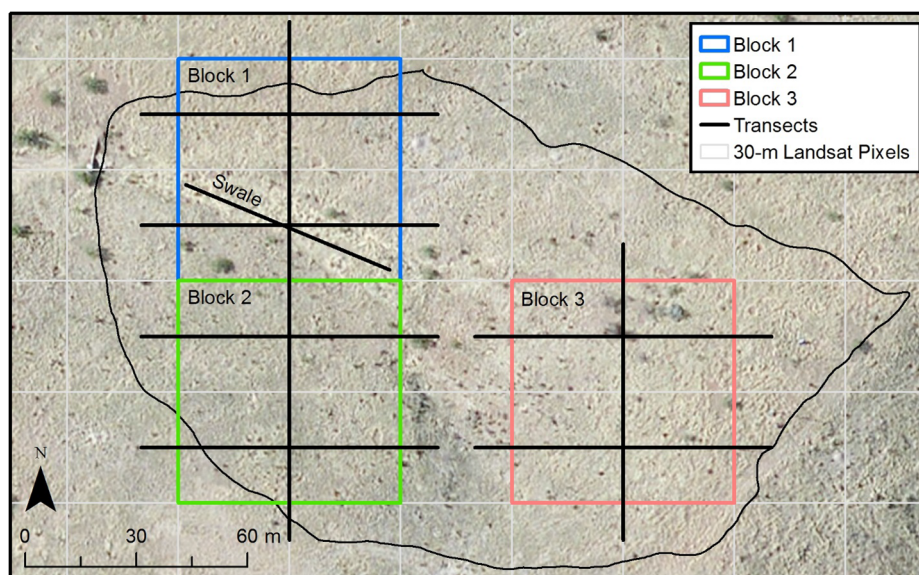


Fig. 3. Transect orientation and study block locations within the Kendall watershed. Approximate Landsat pixel locations are shown in gray. (For interpretation of the references to color in this figure legend, the reader is referred to the web version of this article.)

Table 1

Field data collection dates and Landsat satellite overpass dates (bold dates denote scenes selected for calibration).

Field Site	Field Collection Date	ETM + Overpass Date	OLI Overpass Date
Kendall	4/22/2015	4/15/2015	4/23/2015
Kendall	5/18/2015	5/17/2015	5/25/2015
Kendall	6/22/2015	6/18/2015	6/26/2015
Kendall	7/24/2015	7/20/2015	7/28/2015
Kendall	8/14/2015	8/5/2015	8/13/2015
Kendall	8/28/2015	9/6/2015	8/29/2015
Kendall	9/28/2015	9/22/2015	9/30/2015
Kendall	10/28/2015	10/24/2015	11/1/2015
WG1	12/2/2015	11/25/2015	12/3/2015
WG2	12/2/2015	11/25/2015	12/3/2015
WG3	12/7/2015	12/11/2015	12/3/2015
WG4	12/7/2015	12/11/2015	12/3/2015

transect data to estimate litter and basal cover from foliar cover values. A data set was compiled of foliar, litter, and basal cover values from each transect block (Kendall and WGEW) on all collection dates ($n = 28$). Regression analysis was conducted between foliar cover and basal cover, and foliar cover and litter cover. The resulting Eqs. (4) and (5) were used to estimate basal (BC_{RS}) and litter (LC_{RS}) cover from FC_{RS} .

$$BC_{RS} = 0.37FC_{RS} - 0.18 \quad (4)$$

$$LC_{RS} = 0.25FC_{RS} + 14.04 \quad (5)$$

2.6. Hydrologic modelling environment

A suite of models and tools were used to conduct the precipitation-runoff simulations in this study. The following section briefly describes the tools used and how they were incorporated into the simulation process. In depth documentation can be located at the URLs provided in the sections below.

2.6.1. KINEROS2 (K2)

K2 (<http://www.tucson.ars.ag.gov/kineros/>) is an event-oriented, physically-based model for simulating interception, infiltration, surface runoff, and erosion for small agricultural, rangeland, and urban watersheds (Goodrich et al., 2012; Miller et al., 2007; Smith et al., 1995). Watersheds in K2 are represented as a network of geometrically

simplified, one-dimensional flow elements. Hortonian overland flow elements are represented as rectangular planes or curvilinear surfaces over which runoff is routed into trapezoidal channel elements that cascade to the outlet of the watershed. Infiltration is modeled using the Smith and Parlange (1978) approximation, and kinematic wave equations are used for overland and channel flow. Rainfall can be distributed across elements from multiple gauges and unique parameter sets can be applied to each of the elements, allowing for representation of spatial heterogeneity in the watershed (Miller et al., 2007). K2 was used in this study to route surface runoff from multiple hillslope simulations through a channel network to the outlet of the Kendall watershed at Weir 112.

2.6.2. Automated Geospatial Watershed Assessment tool (AGWA)

Determination of watershed geometry and initial model parameterization were conducted using AGWA version 3.6.1 (www.tucson.ars.ag.gov/agwa/) within the ESRI ArcGIS (version 10.4) environment (Goodrich et al., 2012; Miller et al., 2007). AGWA allows for rapid model parameterization and data propagation from nationally available data sources (e.g., soils, elevation, land cover, and precipitation) within the ArcGIS geospatial environment. Tools within AGWA allow for the delineation of watershed boundaries, discretization of model elements, model parameterization, model execution, and visualization of results. The GIS environment provided the ability to distribute geospatial and remotely sensed data across discrete model elements representing the structure of the watershed.

2.6.3. Rangeland Hydrology and Erosion Model (RHEM)

RHEM is a process-based, hillslope-scale model for estimating runoff and soil loss within rangeland environments (Hernandez et al., 2017; Nearing et al., 2011). RHEM v2.3 is available for use as a web-based decision support tool (<http://apps.tucson.ars.ag.gov/rhem/>) and is incorporated into AGWA to work in conjunction with K2, used for channel routing, to perform watershed-scale simulation. The hydrology component of RHEM is similar to K2, but incorporates unique parameterization equations that utilize quantifiable measures of vegetative and ground cover across multiple vegetative communities (e.g., foliar cover, litter cover, basal cover, rock cover and cryptogam cover). RHEM was developed for use at the hillslope scale as a soil loss estimation tool for use specifically on rangelands.

2.7. Model parameterization

A unique set of model parameters was created for each rainfall-runoff event. Additionally, four parameterization scenarios were evaluated in which a default parameterization in AGWA was compared to three FC_{RS}-based scenarios at varying temporal resolutions. The parameterization procedure within AGWA used to create the default scenario is outlined in Sections 2.7.1–2.7.3. Modifications to this procedure using the remotely sensed data to produce the FC_{RS}-based scenarios are discussed in Section 2.8.

2.7.1. Hydrologic inputs and storm selection

Twenty-six runoff-producing rainfall events occurring in July, August, and September were used for simulation and validation. Precipitation breakpoint data measured at WGEW Raingage 82 were input into RHEM/K2 for each event. Since the model does not have an inter-storm component, an estimate of the pre-storm initial relative soil saturation (SI) is required to quantify the antecedent soil moisture (Goodrich et al., 1994). SI was calculated using volumetric water content (VWC) measurements from the soil moisture sensors located at 5 cm depth near the meteorological station at the beginning of each event. Soil moisture data were not available prior to 1996, which limited the study to the years 1996–2015. Gauged runoff volume and peak flow rate data measured by a V-notch weir at the outlet of the watershed (WGEW Weir 112) were associated with each precipitation event and used as model validation criteria. Only storms in which the ratio of runoff to precipitation was greater than 5% were used for simulation (Table 2). These data are available from the USDA ARS Southwest Watershed Research Center via a web interface at <http://www.tucson.ars.ag.gov/dap/>.

2.7.2. Watershed delineation and discretization

The delineation of the Kendall watershed boundary was performed with the AGWA watershed delineation tool using a LiDAR-based, 0.5 m DEM and the point location of the outlet of the sub-watershed at Weir 112. The watershed was then broken into discrete hillslope and channel

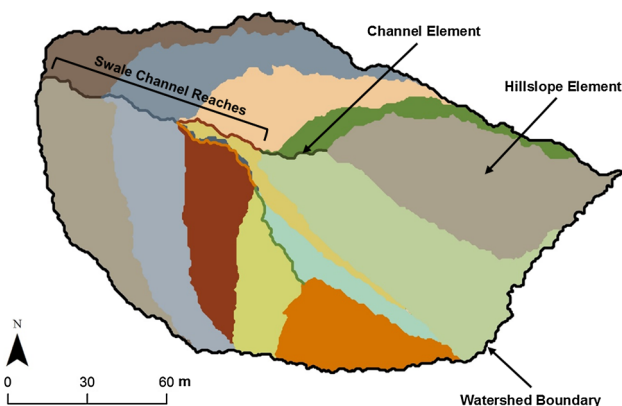


Fig. 4. Hillslope and channel modelling elements for the Kendall watershed. Different colors denote a unique set of model parameters for each hillslope or channel reach. (For interpretation of the references to color in this figure legend, the reader is referred to the web version of this article.)

reach elements using the AGWA discretization tool. Default channel element width and depth are estimated in AGWA using empirical hydraulic-geometry relationships as a function of contributing area for the top and bottom of each channel reach (Miller et al., 2007). The initial AGWA-calculated channel widths at the top and bottom of each reach were refined with field-measured data.

The “user-defined pour points” option was used in AGWA to describe the channel network and create the watershed elements. This method allows the user to manually set the initiation points of channels and subdivide channel reaches with different characteristics using GIS point features. Channel initiation points were placed at the beginning of two main channels that drain into the vegetated swale at the base of the watershed. Internal pour points were placed at the initiation of the swale to separate the two main upland channels from the channel in the swale. The channel within the swale was further subdivided to represent changes in soil type and channel width. Based on the definition

Table 2

Precipitation-runoff events selected for model simulation shown with gauged precipitation and runoff values. I₃₀ is the peak 30-minute rainfall intensity and SI is the relative soil saturation. The runoff ratio is defined as total runoff depth (Q) divided by total precipitation depth (P).

Storm ID	Date	Precipitation				Runoff			
		Duration (min)	Depth (mm)	I ₃₀ (mm/hr)	SI	Depth (mm)	Peak Rate (mm/hr)	Runoff Ratio (–)	
1	8/27/1996	105	26.9	44.3	0.22	6.2	26.1	0.23	
2	7/14/1999	75	23.1	42.3	0.22	2.0	11.8	0.09	
3	7/21/1999	217	28.5	37.9	0.34	2.9	11.8	0.10	
4	7/27/1999	24	8.4	16.8	0.31	0.8	4.3	0.09	
5	8/5/1999	67	11.9	21.5	0.36	2.0	9.2	0.17	
6	9/19/2004	143	17.7	22.1	0.27	0.9	3.4	0.05	
7	8/3/2006	123	19.3	36.3	0.27	5.4	30.5	0.28	
8	8/6/2006	27	16.9	33.8	0.34	4.0	23.6	0.24	
9	8/10/2006	111	27.8	42.8	0.34	9.6	25.1	0.35	
10	8/11/2006	68	17.9	34.9	0.36	8.2	36.7	0.46	
11	8/12/2006	14	4.8	9.7	0.36	0.5	3.0	0.11	
12	8/13/2006	141	11.3	13.3	0.31	2.9	11.6	0.25	
13	8/16/2006	27	7.5	15.0	0.29	1.8	8.1	0.25	
14	8/17/2006	50	10.2	19.0	0.36	3.9	17.9	0.38	
15	9/4/2006	32	8.6	16.9	0.20	0.5	2.8	0.06	
16	7/20/2007	245	57.0	72.6	0.20	14.1	37.6	0.25	
17	7/23/2007	14	9.7	19.3	0.33	1.0	6.6	0.10	
18	8/6/2007	59	12.3	18.3	0.34	0.7	2.8	0.06	
19	8/27/2008	58	38.4	71.6	0.14	10.7	43.3	0.28	
20	8/27/2008	65	28.3	33.5	0.23	4.2	13.7	0.15	
21	8/28/2008	34	28.6	61.0	0.27	12.9	34.9	0.45	
22	8/13/2009	9	9.8	19.6	0.27	2.1	10.2	0.21	
23	8/23/2009	67	28.8	45.0	0.22	1.7	5.6	0.06	
24	7/29/2011	68	30.1	47.0	0.34	3.7	16.6	0.12	
25	9/5/2012	101	33.0	57.2	0.27	7.4	22.9	0.22	
26	7/25/2014	52	32.8	54.6	0.18	2.0	7.0	0.06	

of these pour points, the watershed was broken up into hillslope elements that contributed to each channel reach (Fig. 4).

2.7.3. Initial model parameterization

Once the watershed was split into discrete elements the initial model parameterization for each element was conducted using the AGWA parameterization tool. This tool requires the input of geospatial layers representing soils data, land cover classification, elevation, and vegetation life-form and cover (RHEM only). The resulting parameter file generated from these data sets provided the necessary watershed parameters to execute the RHEM/K2 model.

Soils data were obtained from the NRCS Soil Survey Geographic Database (SSURGO). The SSURGO spatial map was intersected with the watershed to obtain the spatial distribution of soil types. AGWA determines a soil texture for each hillslope element from the SSURGO tabular data using a weighting scheme based on spatial distribution of soils within an element; proportion of soil components within a complex; and soil horizons to 22.9 cm depth (Miller et al., 2007). The textural classification (USDA) of the soil across Kendall was described as a sandy clay loam, composed of 46.7% sand, 23.0% silt and 30.3% clay. This texture was applied to all hillslope elements. Soil parameters including saturated hydraulic conductivity (K_b), percent rock, suction head, and porosity were estimated based upon the soil texture classification using pedo-transfer functions, lookup tables, and algorithms within AGWA. (Hernandez et al., 2017; Rawls et al., 1982; Rawls et al., 1998).

Channel elements are given default soil characteristic and hydraulic roughness parameters values based upon the assumption of a sandy bed. This assumption produces high transmission losses within the channel (Miller et al., 2007). The two upland channels were not incised and no noticeable change in soil texture or vegetation composition from the adjacent hillslopes was seen, therefore the same soil texture used for adjacent hillslope elements was applied to these channel elements. The channel reaches in the swale region contained large amounts of coarse sediment deposition, creating a sandy upper horizon. The soil texture for these reaches was left defined as a sand soil texture class.

Land cover classification was defined using the 2011 National Land Cover Database (NLCD). The NLCD is a Landsat-derived land cover classification map covering the conterminous United States. Each 30 m pixel is classified as one of sixteen land cover classes, consistent with previous NLCD releases (Homer et al., 2015). A lookup table in AGWA associates a literature based foliar cover value (in this case 25%) and an associated interception depth parameter value with each land cover class. Canopy interception (I_n) in RHEM/K2 is reflected as the average depth of rainfall captured by the vegetation on a hillslope. The I_n parameter is calculated by reducing the rainfall rate by the cover fraction (based on percent foliar cover, FC_{RS} , in this study) until the amount retained reaches the user defined maximum interception depth (Smith et al., 1995). This value was applied to all hillslope elements.

Plant community, foliar, basal, litter, rock and cryptogamic cover values are needed to calculate the effective saturated hydraulic conductivity (K_e) and the Darcy friction factor (f_t) parameters in RHEM. The K_e parameter modifies the initial estimate of saturated hydraulic conductivity (K_b) based on soil texture, as outlined above, to account for the effects of increased infiltration with an increase of vegetative cover or change in composition (Hernandez et al., 2017; Nearing et al., 2011). The K_e parameter is calculated as:

$$K_{e_i} = K_{b_i} e^{[p_i(litter+basal)]} \quad (6)$$

where K_{b_i} is the 25% percentile saturated hydraulic conductivity for each soil textural class (i); p is the natural log of the ratio of the 75% to the 25% percentile values of saturated hydraulic conductivity; *litter* is percent litter cover; and *basal* is percent basal cover (Hernandez et al., 2017). This parameter is further adjusted by applying a multiplier based on the dominant plant life-form (e.g., bunch grass: 1.0, sod grass:

0.8, forbs: 1.0, shrub: 1.2). The f_t parameter represents hydraulic roughness in RHEM. It incorporates ground cover and slope measurements and has been shown to be negatively correlated with bare ground, with basal cover being the most influential ground cover factor (Al-Hamdan et al., 2015). The f_t parameter is calculated as:

$$\log(f_t) = -0.109 + 1.425litter + 0.442rock + 1.764(basal + crypto) + 2.068S, \quad (7)$$

where *litter* is the fraction of area covered by litter to total area ($m^2 m^{-2}$); *rock* is the fraction of area covered by rock cover to total area ($m^2 m^{-2}$); *basal + crypto* is the fraction of area covered by basal plus cryptogam cover to total area ($m^2 m^{-2}$); and S is slope ($m m^{-1}$) (Al-Hamdan et al., 2015).

The plant life-form group for Kendall was defined as bunch grass dominated, determined from field observations. Transect-measured rock cover was applied to individual elements based on the element's proximity to a given transect and remained static for all simulations. Cryptogam cover did not exist in the watershed and was assigned a null value. Basal and litter cover were calculated by applying Eqs. (4) and (5) to the foliar cover value obtained from the NLCD lookup table.

This set of parameters defined using AGWA and the literature-based foliar cover value served as the *a priori* parameterization scenario (Scenario 1) for all precipitation-runoff simulations. Additional model calibrations were performed using the remotely sensed data, wherein the foliar cover value used in Scenario 1 was replaced with Landsat-based FC_{RS} values. The intrinsic characteristics of the watershed (e.g., topography, watershed geometry, porosity) were left as static values for all event simulations. However, the I_n , K_e , and f_t parameters in RHEM/K2 were altered using FC_{RS} and the derived BC_{RS} , and LC_{RS} data.

2.8. Model parameterization integrating remotely sensed foliar cover

Three additional parameterization scenarios were developed using the FC_{RS} time series. The three FC_{RS} -based scenarios (Scenarios 2–4) were designed to evaluate the effects of temporal variability of foliar cover on model performance, as well as to assess the value of spatially localized data in comparison to Scenario 1.

Foliar cover values were calculated for each hillslope element by using a weighted average of all intersecting 30 m Landsat pixels within the boundary of the element. Basal and litter cover were calculated using Eqs. (4) and (5) using the mean foliar cover value from each hillslope element. These values were then input into the RHEM parameterization Eqs. (6) and (7) to calculate K_e , and f_t and the foliar cover value was applied to I_n . The remaining static parameters for each hillslope and channel element were calculated as outlined in the previous section.

Scenario 2 was based on a long-term mean foliar cover value from 1996 to 2015, representing the assumption that foliar cover during the growing season remained constant over time. The mean of FC_{RS} values between July and September of each year were calculated. The mean of these values was then calculated, resulting in a static, long-term estimate of foliar cover for the study period. The long-term mean was calculated in this fashion in order to minimize the influence of the varying number of images available during the monsoon period each year. This calculation was performed for each Landsat pixel intersecting Kendall, resulting in a spatially distributed grid of foliar cover values.

Scenario 3 was based on an annually varying mean foliar cover value, representing the assumption that foliar cover remained constant during any given monsoon season, but varied between years. This value was determined by taking the mean of all FC_{RS} values between July and September of each year. This resulted in a dynamic series of 15 annual foliar cover grids that were then associated with all precipitation events that occurred in that year.

Scenario 4 was the most temporally localized of the three FC_{RS} -based scenarios. FC_{RS} values acquired within the closest temporal proximity to a selected precipitation event were associated with that

event. No FC_{RS} images were acquired more than 10 days before or after a given precipitation event.

2.9. Model execution and performance evaluation

RHEM/K2 precipitation-runoff simulations were executed for all selected events (Table 2) using the four parameterization scenarios. Runoff volume and peak flow rate for all storms were evaluated as a lumped data set, including the values from all 26 simulated events. The RMSE-observations Standard Deviation Ratio (RSR) and Percent Bias (PBIAS) were the performance metrics used in this study, as outlined by Moriasi et al. (2007). RSR standardizes the RMSE with the standard deviation of the observed data, with an optimum value of 0. RSR is calculated as:

$$RSR = \frac{RMSE}{STDEV_{obs}} = \frac{[\sqrt{\sum_{i=1}^n (Y_i^{obs} - Y_i^{sim})^2}]}{[\sqrt{\sum_{i=1}^n (Y_i^{obs} - Y^{mean_{obs}})^2}]}, \quad (8)$$

where Y_i^{obs} is the i th observation of the measured data, Y_i^{sim} is the i th observation of the simulated data, and $Y^{mean_{obs}}$ is the mean of the observed data (Moriasi et al., 2007). PBIAS is a measure of the tendency of a model to over- or under-estimate values compared to the observed data (Gupta et al., 1999). PBIAS is calculated as:

$$PBIAS = \left[\frac{\sum_{i=1}^n (Y_i^{obs} - Y_i^{sim}) * 100}{\sum_{i=1}^n (Y_i^{obs})} \right], \quad (9)$$

where Y_i^{obs} is the i th observation of the measured data and Y_i^{sim} is the i th observation of the simulated data. The optimal value of PBIAS is 0, with values of lower magnitude representing more accurate simulation. Positive values indicate a model underestimation bias and negative values indicate a model overestimation bias.

3. Results and discussion

3.1. Field-based characterization of the watershed

The invasive *Eragrostis lehmanniana* (Lehmann lovegrass) was the dominant species measured within all Kendall transect blocks (68% of watershed vegetation). Other species with notable presence were: *Hilaria belangeri* (Steud.) Nash (curly-mesquite grass) (14%); *Calliandra eriophylla* Benth. (fairyduster) (3%); *Bouteloua curtipendula* (Michx.) Torr. (sideoats grama) (3%); *Acacia constricta* Benth. (whitethorn acacia) (2%); and *Pleuraphis mutica* Buckley (tobosagrass) (2%). All other species present represented less than one percent of the total vegetative composition and were comprised of annual forbs, perennial grasses, shrubs, and cactus. Composition for the three study blocks were similar, with Lehmann lovegrass dominating the composition, followed by native grasses, shrubs, and forbs. The vegetative composition within the swale differed slightly from the uplands in the watershed with a greater amount of annual forbs (17%) and less native grass (4%) compared to 2% and 22% respectively in the uplands.

Foliar cover on Kendall (mean value of Block 1, Block 2, and Block 3) ranged from 63% on 6/22/2015 to 82% on 9/28/2015 (Fig. 5). The annual mean foliar cover on Kendall spanning the growing season was 73% ($s = 6\%$). Lehmann lovegrass inflorescences were first observed on 8/14/2015 and were widespread by the 8/28/2015 collection date. The large panicle inflorescences mainly accounted for the increased measure of foliar cover seen in August and early September. The three Kendall blocks and the swale transect maintained similar foliar cover values throughout the collection period.

While total foliar cover remained relatively stable over the course of the growing season, the green and senescent components showed greater variability. The vegetation was predominantly senescent until the 7/24/2014 collection date (Fig. 5). Green vegetation during this period was composed of annual forbs and Lehmann lovegrass.

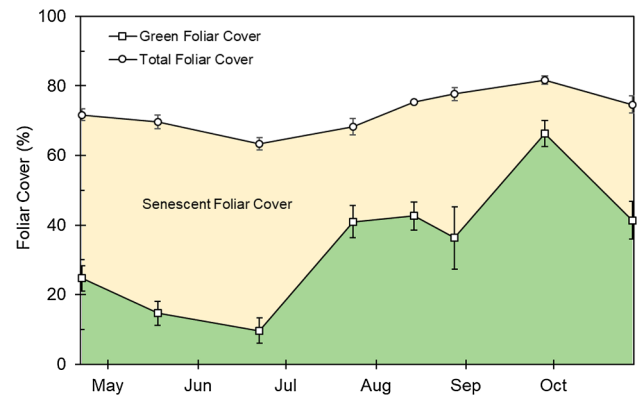


Fig. 5. Mean foliar cover of the Kendall study blocks over the 2015 monsoon season. Error bars denote standard deviation. While total foliar cover remained relatively constant, the green and senescent components varied over the course of the season. (For interpretation of the references to colour in this figure legend, the reader is referred to the web version of this article.)

Vegetation greenness responded to the onset of monsoon precipitation occurring in late June. Greenness stabilized with intermittent rainfall and peaked after a large pulse of precipitation in early September. Consistently elevated green foliar cover values were observed in the swale transect due to the increased presence of forbs and improved plant available water from upland drainage.

Basal cover was similar between all blocks and remained relatively constant over the collection period ($\bar{x} = 27\%$, $s = 6\%$) with only a slight increasing trend visible after the 6/22/2015 monitoring (Fig. 6). The swale contained slightly lower basal cover values due to a high presence of forbs. Litter cover also remained relatively constant for the three Kendall blocks with a slight decrease over the growing season [$\bar{x} = 33\%$, $s = 4\%$] (Fig. 6). The swale contained significantly higher litter cover (t -test, $p < 0.05$) on all collection dates ($\bar{x} = 59\%$, $s = 6\%$). Mean rock cover ($\bar{x} = 24\%$, $s = 4\%$) was significantly higher (t -test, $p < 0.05$) in the three study blocks than in the swale [$\bar{x} = 5\%$, $s = 3\%$] (Fig. 6).

Foliar cover was the most dynamic variable with a slight increase in foliar cover near peak productivity caused by inflorescence growth. However, from a hydrological perspective, this small change in foliar cover would only affect rainfall interception and have a minimum effect on surface runoff produced from high-intensity monsoon rainfall. The results also show the importance of sufficient spatial coverage of transect measurements for representing changes in soils and vegetation composition. Although little spatial variability was seen in the vegetative composition or ground cover measurements in the uplands of the

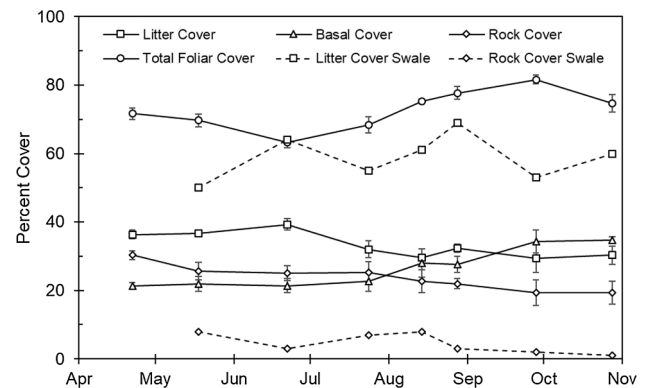


Fig. 6. Mean foliar and ground cover for the Kendall blocks (solid lines) and significantly different (t -test, $p < 0.05$) swale transect cover measurements (dotted lines). Only rock and litter cover in the swale were significantly different from those in the uplands.

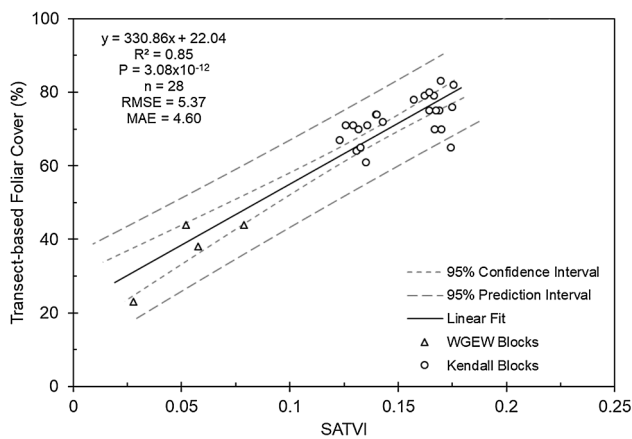


Fig. 7. Regression analysis between the best performing vegetation index values, the Soil Adjusted Total Vegetation Index (SATVI), and field-measured foliar cover for all study blocks and collection dates.

watershed, significant differences were seen in the swale. Increased litter and decreased rock cover, as well as altered vegetative composition, in the swale indicated that different hydrologic properties exist in this portion of the watershed and need to be accounted for in runoff simulation as K_e and f_t (Eqs. (6) and (7)) are functions of these RHEM inputs.

Field measured basal and litter cover remained relatively static over the course of the 2015 growing season, while foliar cover was more dynamic. Application of Eqs. ((4) and (5)) at a sub-annual frequency could introduce unrealistic fluctuations in the amount of basal and litter cover. To best represent the static nature of these vegetative components, a mean annual value or singular value taken near peak productivity is recommended.

3.2. Landsat-based foliar cover calibration

Results from the regression analysis between the vegetation indices and field measured foliar cover indicated that SATVI (Fig. 7) was the best predictor of total foliar cover ($R^2 = 0.85$, $RMSE = 5.37$, and $MAE = 4.60$) compared to NDVI ($R^2 = 0.66$, $RMSE = 8.10$, and $MAE = 6.61$) and SAVI ($R^2 = 0.57$, $RMSE = 9.07$, and $MAE = 7.38$). This result is consistent with Hagen et al. (2012) which showed SATVI to be the best performing vegetation index of those evaluated across western rangeland sites. However, the resulting Eq. (10) from the regression analysis differed from the broad-scale rangeland equation developed in Hagen et al. (2012) which underestimated foliar cover in this localized grassland environment.

$$FC_{RS} = 330.86SATVI + 22.04 \quad (10)$$

The regression analysis reinforces the observations from the intra-annual vegetation measurements in that herbaceous vegetation within semiarid grasslands may only be green for a portion of the year. Therefore, spectral remote sensing techniques must account for both green and senescent vegetation to accurately quantify total foliar cover. Greater uncertainty exists in FC_{RS} values below 60% and above 80% as the dataset is largely composed of calibration data from the Kendall blocks which fell within this dynamic range. This relationship was developed using foliar cover values within a localized grassland community and therefore, cannot be applied with a high degree of certainty to landscapes containing different plant communities.

3.3. Allometric relationships for basal and litter cover estimation

The linear relationship between foliar and basal cover showed significant ($R^2 = 0.57$, $p < 0.05$) correlation (Fig. 8). The relationship makes physical sense within this bunchgrass dominated vegetation

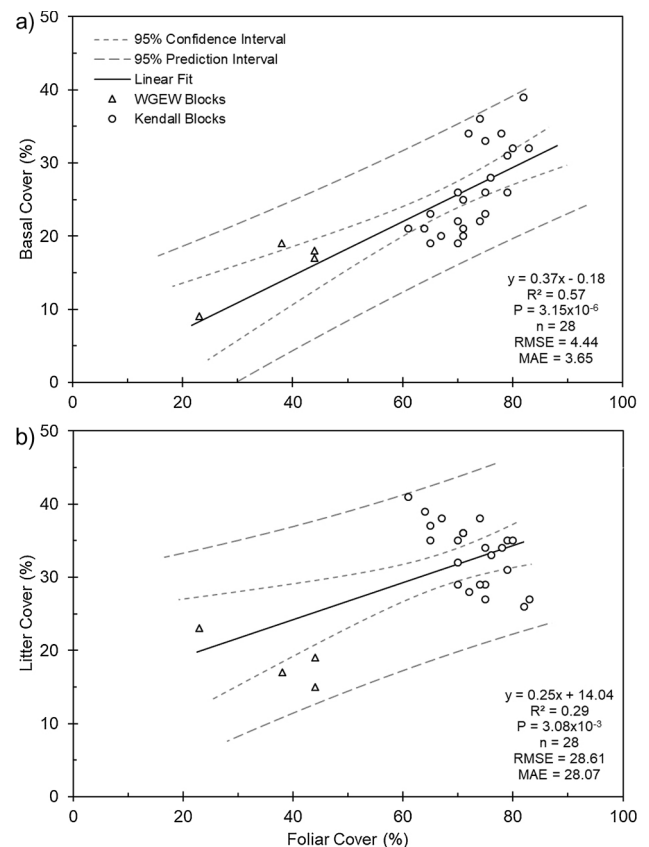


Fig. 8. Linear regression between a) foliar cover and basal cover values and b) foliar cover and litter cover values from all study blocks and collection dates.

community in that an increase of basal area would result in an increase in foliar cover with zero basal cover resulting in approximately zero foliar cover ($b = -0.18$). The correlation between foliar and litter cover was weak, but significant [$R^2 = 0.29$, $p < 0.05$] (Fig. 8). This relationship is generalized and is based on the assumption that with greater amounts of foliar cover, a greater potential for litter cover exists. The relationship ignores many complex physical and temporal factors that affect litter presence over time. Furthermore, while the swale contained a significantly higher amount of litter than the uplands, the equation shown in Fig. 8 was applied to all model elements for simplicity. Additional, long-term data collection is required to develop more robust models for these relationships. However, these simple relationships provide a conceptual foundation for research in this context moving forward.

3.4. Landsat-based foliar cover time series

The FC_{RS} time series produced by the application of Eq. (10) is shown in Fig. 9. The lower image frequency occurring from 1996 to 1999 and in 2012 was the result of only one Landsat satellite in orbit during that period. Better representation of phenology and periods of peak productivity were seen in the periods where two satellites were in orbit. However, high frequency variability between consecutive FC_{RS} values was apparent in periods where foliar cover was below 60%. This may be a result of differences between satellite measurements (e.g., Landsat 5 and Landsat 7 or Landsat 7 and Landsat 8) or physical changes in vegetation or moisture content. Further research needs to be conducted to determine the source of this variability. A cross-platform calibration of bands would need to be done if the variability is sourced to differences in satellite measurements.

Evidence of the drought-induced vegetation change in which the watershed was occupied by forbs in 2006 and transitioned to a

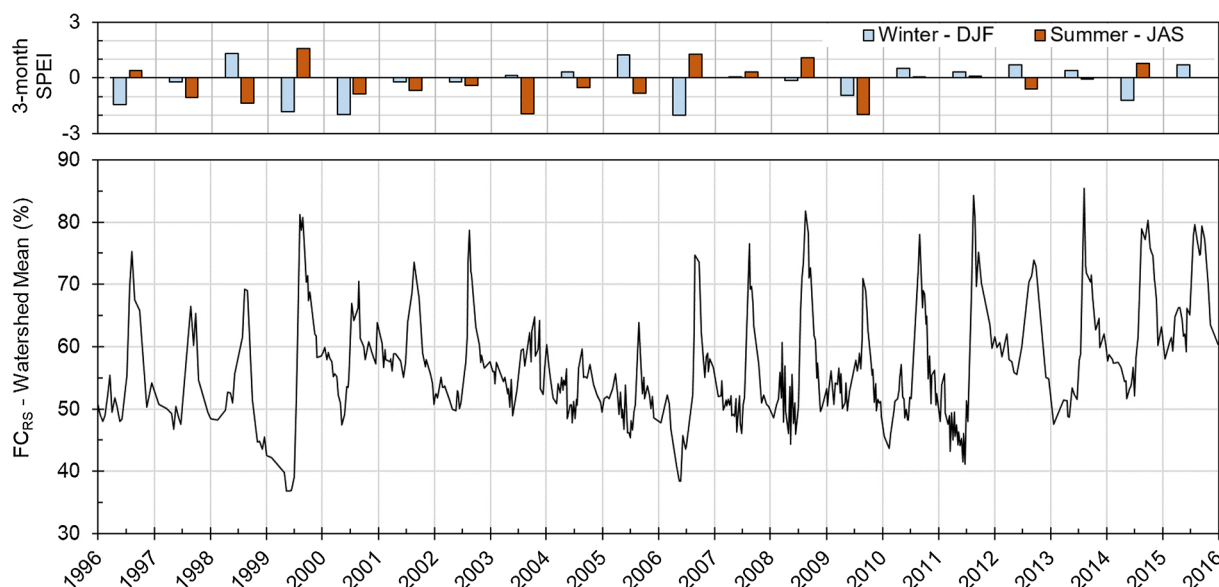


Fig. 9. Time series of remotely sensed foliar cover (FC_{RS}). The values shown are a spatial average of all pixels intersecting Kendall. Three-month summer and winter Standardized Precipitation-Evapotranspiration Index (SPEI) values are shown for context. Positive values of increasing magnitude indicate increasingly wetter conditions. Negative values of increasing magnitude indicate increasingly dry conditions. SPEI values are based on a record from 1901 to 2014 and provided at a 0.5° spatial resolution (Vicente-Serrano et al., 2010). Data were accessed from the Global SPEI Database (<http://sac.csis.es/spei/database.html>).

Lehmann lovegrass dominated grassland can be seen in the FC_{RS} time series (Fig. 9). Beginning in 2000, a succession of dry years with below average winter (2000–2003) and monsoon precipitation (2000–2005) and high temperatures occurred. Following a late flush of vegetation productivity in 1999, a decreasing trend in foliar cover was present, reaching a low point of $< 40\%$ in the spring of 2006 (Fig. 9). This trend is consistent with observed reduced net ecosystem carbon uptake, an indicator of lower productivity, during these years (Emmerich, 2003; Scott et al., 2010). Despite above average monsoon precipitation from 2006 to 2008, native species did not fully recover, were replaced with a flush of annual grasses and forbs in 2006, which was succeeded by Lehmann lovegrass thereafter (Scott et al., 2010).

Nine of the twenty-six runoff events used in this study occurred during the 2006 monsoon. Precipitation intensities were not abnormally high for these events, but runoff ratios were generally elevated during this period (Table 2). Soil erosion resulting from these events accounted for 42% of the 19-year sediment loss record (Polyakov et al., 2010). The coincidence of change in vegetation and the spike in runoff and sediment loss suggest a drastic change in watershed response. Minimum plant litter was measured in 2007 (Scott et al., 2010) and the presence of annual vegetation allude to decreased basal cover during this period. Increased flow velocities and decreased infiltration rates can be expected from these conditions resulting in higher runoff and erosion.

While not as well documented as the vegetation die-off in 2006, a similar response from extremely low to high FC_{RS} values within a growing is shown in 1999 (Fig. 9). Historic composition data shows a spike in forb presence in 1999 similar to that of 2006. High annual forb cover and a decrease in FC_{RS} leading up to 1999 suggest a similar period of grass die-off. Further data collection needs to be conducted to validate FC_{RS} during these periods of altered vegetation composition.

After 2006 a general increasing trend in foliar cover is present (Fig. 9). Lehmann lovegrass has largely dominated the watershed's vegetation since 2008. While the grass species present on the watershed have changed, foliar cover appears to have returned to historic levels. In the period from 2008 to 2015, only 8 significant runoff events occurred (runoff ratio greater than 5%), including 3 events in 2008 when the grass vegetation was dominated by seedlings (Table 2). The infrequency of runoff events in recent years and high foliar, litter, and

basal cover measurements suggest that the watershed is hydrologically stable under this vegetative state.

3.5. Foliar cover input scenarios

The remotely sensed foliar cover values based on FC_{RS} (Scenarios 2–4) were higher than the NLCD-based value (Scenario 1) of 25% in all cases (Fig. 10). Regardless of the temporal resolution, the remotely sensed data more closely resembled that of the field-measured data, reinforcing the importance of spatially localized data. The cover values shown in this section are based on a spatial average of all pixels within the domain of the watershed for discussion purposes.

Scenario 2 (long-term mean of FC_{RS} from 1996 to 2015) represented a static FC_{RS} value of 65% and derived BC_{RS} and LC_{RS} values of 24% and 30% respectively, compared to the corresponding values of 25%, 9%, and 20% in Scenario 1. These static values were applied to all 26 simulation events.

Scenario 3 (annual FC_{RS} means) showed improved representation of inter-annual fluctuation compared to Scenarios 1 and 2, and general trends in FC_{RS} response to climatic variability were visible. FC_{RS} , BC_{RS} , and LC_{RS} values for Scenario 3 ranged from 58%, 21%, and 29% in 2006 to 73%, 27%, and 32% in 2008 respectively. Phenological timing and image availability had a large impact on the annual FC_{RS} means. The timing of vegetation green-up, where FC_{RS} values were largest, was highly variable between years. The annual mean FC_{RS} value can be inflated if this green up occurs early, due the inclusion of more high values in the calculation of the mean (between July and September). Similarly, the number of available cloud-free images and the dates they are acquired can affect the annual mean FC_{RS} value.

Scenario 4 values (FC_{RS} value closest to the event date) allow for representation of intra-annual variability and may be higher or lower than Scenarios 2 and 3 values within a given year. The greatest variability of values associated with a runoff event occurred in 1999. FC_{RS} , BC_{RS} , and LC_{RS} values ranged from 52%, 20%, and 27% respectively on 7/16/1999 to 81%, 30%, and 34% on 9/9/1999. The determination of BC_{RS} and LC_{RS} from FC_{RS} for model parameterization using intra-annual values may be problematic as unrealistic increases in these values could occur within a year, contradicting the static nature of basal and litter cover the 2015 transect data suggested (Fig. 5).

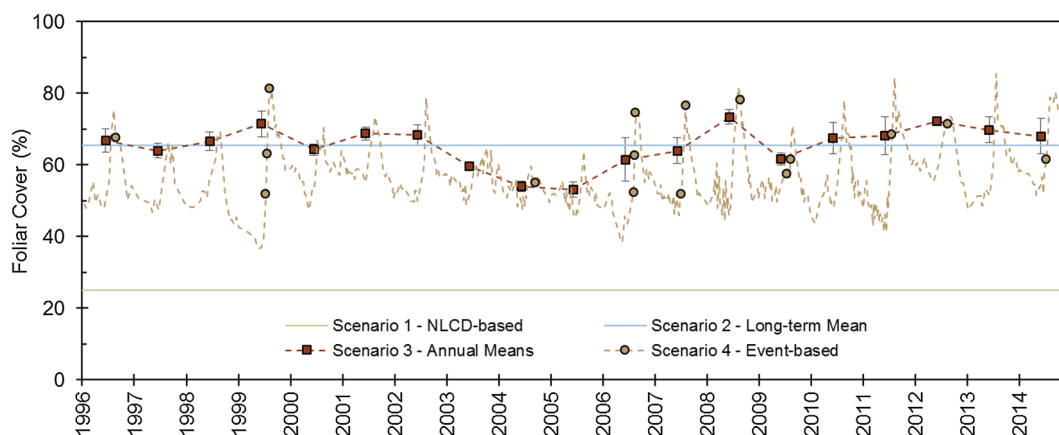


Fig. 10. NLCD-based and FCRS foliar cover input scenarios used for RHEM/K2 parameterization (1996–2014). Error bars show standard error.

3.6. Runoff simulation and model evaluation

The mean simulated runoff volume for the 26 event, lumped data set was greater than that of the observed dataset, but more accurate for the remotely sensed scenarios (Table 3). Negative PBIAS in all cases indicated model over-estimation of total runoff volume. However, smaller PBIAS values were shown in Scenarios 2–3 than for Scenario 1 (−113.27), with Scenario 3 having the smallest PBIAS (−50.33%). RSR values were also improved using the remotely sensed data value, with Scenario 3 performing best (0.77) and Scenario 1 performing the worst (0.95). Moriasi et al. (2007) suggest streamflow model evaluation criteria for satisfactory performance of ± 25% for PBIAS and 0.70 for RSR. These values may be inappropriate for event-based data, but serve as a generalized benchmark here. Overall, model accuracy measures were improved with the incorporation of FC_{RS}, with the best PBIAS and RSR values shown for Scenario 3 (Table 3).

Agreement between the observed and simulated peak flow rates data sets were better than those for total runoff volume. Scenario 1 showed model overestimation with a simulated mean peak runoff rate of 25.72 mm/hr compared to an observed mean of 16.43 mm/hr and PBIAS of −56.56% (Table 3). The remotely sensed scenarios showed little bias, with PBIAS values less than a magnitude of 5%, with Scenario 3 performing best (0.37%). Smaller RSR values for Scenarios 1–3 indicated better model performance for Scenarios 1–3 compared to Scenario 1 (0.83), with Scenario 3 performing best (0.70). Based on the

Table 3

Descriptive statistics and performance metrics for the subset of 26 events that were simulated, total runoff volume (top) and peak runoff volume (bottom), are shown and categorized by the four foliar cover input scenarios. Simulated means were not shown to be statistically significantly different (Tukey HSD, P < 0.05).

Total Runoff Volume (mm)	Scenario 1	Scenario 2	Scenario 3	Scenario 4
Standard Deviation (Obs.)	3.92	3.92	3.92	3.92
Standard Deviation (Sim.)	8.25	7.03	6.83	6.95
Mean (Obs.)	4.32	4.32	4.32	4.32
Mean (Sim.)	9.21	6.67	6.49	6.72
R ²	0.53	0.54	0.54	0.53
RSR	0.95	0.78	0.77	0.79
PBIAS (%)	−113.27	−54.53	−50.33	−55.66
Peak Runoff Rate (mm/hr)	Scenario 1	Scenario 2	Scenario 3	Scenario 4
Standard Deviation (Obs.)	12.31	12.31	12.31	12.31
Standard Deviation (Sim.)	20.95	17.35	16.61	16.77
Mean (Obs.)	16.43	16.43	16.43	16.43
Mean (Sim.)	25.72	16.87	16.37	17.16
R ²	0.53	0.50	0.50	0.50
RSR	0.83	0.71	0.70	0.71
PBIAS (%)	−56.56	−2.71	0.37	−4.47

performance metrics, Scenario 3 produced the best simulated peak runoff rate results.

Slopes and intercepts for runoff volume and peak flow regressions were not shown to be significantly different (ANCOVA, α = 0.05) between the four scenarios (Fig. 11). However, relative improvement in RSR and PBIAS for both simulated runoff volume and peak flow were shown using the remotely sensed foliar cover inputs (Table 3). Negligible differences in performance were seen between Scenarios 2–4. Based on the model performance metrics (Table 3) and the analysis of the field-measured cover data it was concluded that annual implementation of FC_{RS}, Scenario 3, was most appropriate for model parameterization.

The comparatively better results for peak flow rate infer that estimates of f_t were better than those of saturated hydraulic conductivity (K_e) in this watershed. One factor that likely affected the overestimated runoff volume was the characterization of the swale. The slope, soil, and ground cover in this area are different from the surrounding hillslopes. Years of sediment deposit in this shallow-sloped region have produced a coarse, sandy soil texture to depths of at least 1 m. These conditions have allowed for altered vegetation and significantly higher litter content. The soil texture in the swale channel elements were modified to represent a sandy texture within the model. However, improved, localized soil data is needed to represent the heightened infiltration in this region of the watershed as soil textural data obtained from SSURGO soils maps may not represent the actual near surface soil texture on the Kendall watershed. These texture classes are the basis for deriving K_b that is then modified by vegetation to calculate K_e (Eq. (6)). Furthermore, the increased litter content seen in the swale transect was not reflected in the FC_{RS} parameterization data which accounts for an underestimation of K_e and overestimation of runoff volume (Hernandez et al., 2017).

Further insight was gained when the simulation results were subset into vegetative life-form groups, i.e., forb-dominated (1999, 2007, and 2007) and grass-dominated (all other years), for visualization purposes (Fig. 11). Increased model overestimation for runoff volume was seen in all scenarios for events that occurred when the watershed was grass-dominated. Overestimation for grass-dominated events was reduced with remotely sensed foliar cover input. The overestimation of runoff occurring in grass-dominated events suggests that K_e is too low under grass-dominated conditions and current soil texture. Distinct differences in the simulated peak flow rate were also seen between vegetation groups. Model overestimation of peak flow rates occurred for grass-dominated events, while underestimation was seen in forb-dominated events. Peak flow rate is largely affected by f_t , which suggests that this parameter is too low under grass-dominant conditions and too high under forb-dominated conditions. These results indicate that the SATVI to foliar cover relationship and allometric relationships used to calculate basal and litter cover here should be modified to represent specific

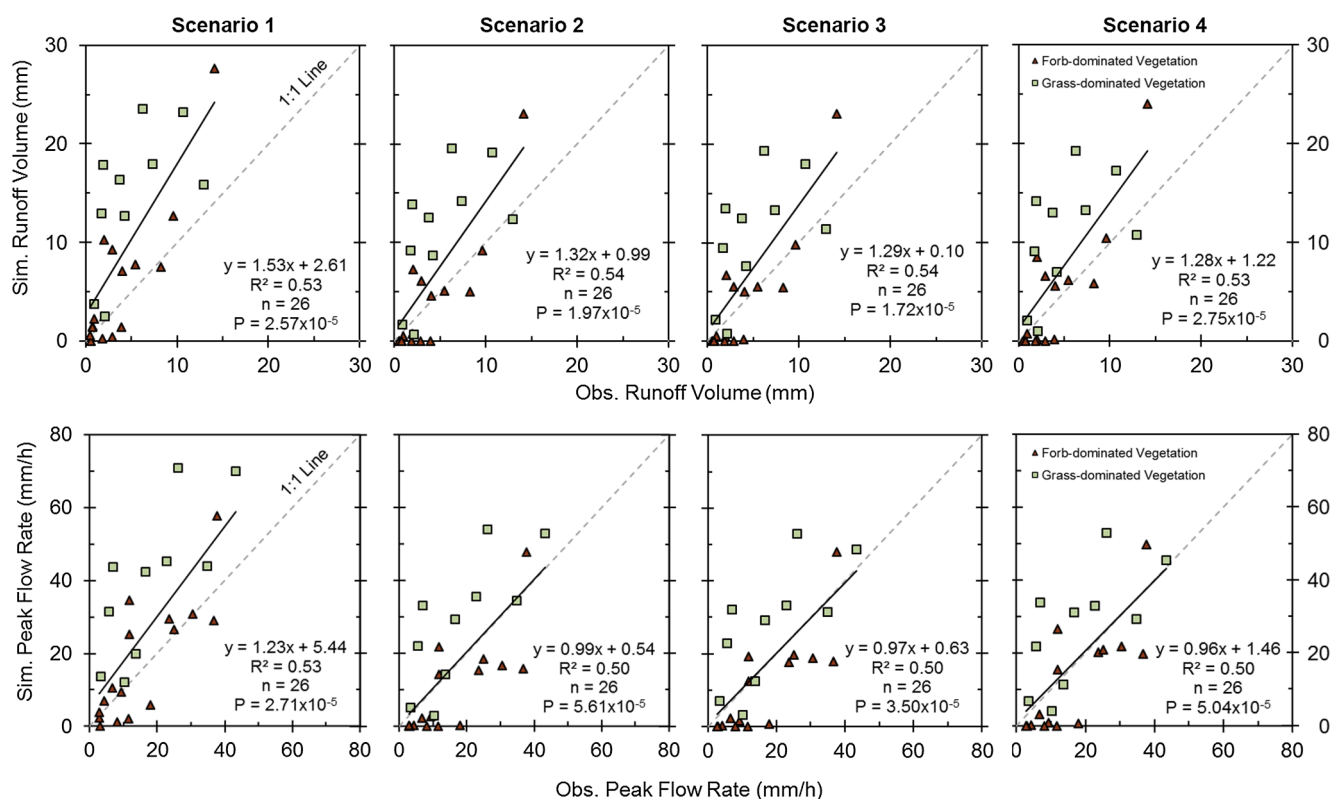


Fig. 11. Regression plots comparing simulated total runoff volume (top row) and simulated peak flow rates (bottom row) with observed values for all precipitation-runoff events. Columns 1–4 represent the different parameterization scenarios.

plant communities. Furthermore, the allometric relationships between foliar cover and litter used here are rudimentary and need to be improved upon through additional data collection and research. The K_e and f_t parameters are sensitive to these inputs and largely affect the model results. Improved understanding of these complex relationships would extend the value of the approach outlined in this research and could further improve model simulation results.

The ability to group the simulated runoff events by dominant vegetation was a luxury due to historic species monitoring on the watershed. Operationally, this type of data may not be available. The use of remotely sensed foliar cover estimates for the parameterization of RHEM/K2 improved simulation results compared to Scenario 1. However, results suggest that in addition to detecting the abundance of vegetation, it is also necessary to detect the type of vegetation. Villarreal et al. (2016) showed success in discerning annual forbs, Lehmann lovegrass, and native grasses using NDVI and SATVI. Implementation of a similar approach could further improve model parameterization by associating a plant community classification with FC_{RS} values.

4. Conclusion

The vegetative composition of the Kendall grassland watershed in 2015 was dominated by the invasive, Lehmann lovegrass. Total foliar cover, basal cover, and litter cover values remained relatively stable throughout the course of the growing season. High variability in green and senescent foliar cover was observed over the measurement period. Due to this fact, the use of SATVI was determined most appropriate for calibrating field measured foliar cover with Landsat imagery due to its ability to detect green and senescent vegetation. The resulting time series of remotely sensed foliar cover showed the ability to detect climate-based alterations in vegetative cover based on a qualitative comparison.

The integrated RHEM/K2 model was parameterized using foliar

cover values from four input scenarios. The first scenario used a literature based value, while the other three were based on the remotely sensed foliar cover values of different temporal representation. Improvement in model performance was seen when the model was parameterized using the remotely sensed data for runoff volume and peak flow rate. Temporal resolution (long-term, annual, and sub-annual) had negligible effect on the simulated values. However, based on the static nature of field observations of foliar, basal, and litter cover over a growing season and slightly better model performance the annual mean value of FC_{RS} , Scenario 3, was selected as the optimum parameterization scheme. These results highlighted the importance of spatially localized vegetation data for model parameterization.

A well-documented change in vegetation on Kendall occurred during the period of simulated events. The vegetation transitioned from native grass-dominated to forb-dominated to its current state of invasive grass dominated. Runoff volume for grass-dominated events were over-predicted by the model to a greater extent than the forb-dominated events. Similarly, simulated peak flow rate was over-estimated for grass dominated events and underestimated for forb-dominated events.

These results emphasize the importance of not only quantifying the abundance of vegetation, but also the type of vegetation. Future research should focus on expanding on the methodologies outlined here to address different vegetation communities. The development of community-specific vegetation relationships between the vegetation index and foliar cover as well as improved basal and litter cover estimates could provide better parameter estimates. However, classification of vegetation communities using remotely sensed data will be required for operational implementation of these improvements.

The research presented in this study provides a framework for the parameterization of the RHEM/K2 model using Landsat-based estimates for required vegetative inputs. While model performance metrics were lower than desired, this methodology shows improvement over the default method of associating literature-based values with geospatial

land cover classes. Furthermore, no parameter optimization or use of calibrated multipliers were used to refine parameter estimates. This allows for improved operational use when data is scarce. This methodology shows the potential for long-term change analysis at the watershed scale and may be especially useful for detecting changes in watershed response based on vegetation disturbances.

Declaration of Competing Interest

None.

Acknowledgements

The authors would like to thank the staff of the USDA ARS Southwest Watershed Research Center for maintenance of the WGEW. Much appreciation to Shea Burns, Mariano Hernandez, Carl Unkrich, and Haiyan Wei for model expertise and assistance. The authors also wish to thank the three anonymous reviewers whose comments and suggestions helped improve and clarify this manuscript. This work was funded in part by the USDA Natural Resources Conservation Service Conservation Effects Assessment Project (CEAP). USDA is an equal opportunity provider and employer. Mention of a proprietary product does not constitute endorsement by USDA and does not imply its approval to the exclusion of the other products that may also be suitable.

References

- Al-Hamdan, O.Z., Pierson, F.B., Nearing, M.A., Williams, C.J., Stone, J.J., Kormos, P.R., Boll, J., Wetz, M.A., 2013. Risk assessment of erosion from concentrated flow on rangelands using overland flow distribution and shear stress partitioning. *Trans. ASABE* 56 (2), 539–548.
- Al-Hamdan, O.Z., Hernandez, M., Pierson, F.B., Nearing, M.A., Williams, C.J., Stone, J.J., Wetz, M.A., 2015. Rangeland hydrology and erosion model (RHEM) enhancements for applications on disturbed rangelands. *Hydrol. Process.* 29 (3), 445–457.
- Al-Hamdan, O.Z., Pierson, F.B., Nearing, M.A., Williams, C.J., Hernandez, M., Boll, J., Nouwakpo, S.K., Wetz, M.A., Spaeth, K., 2017. Developing a parameterization approach for soil erodibility for the Rangeland Hydrology and Erosion Model (RHEM). *Trans. ASABE* 60 (1), 85–94.
- Asner, G.P., Archer, S., Hughes, R.F., Ansley, R.J., Wessman, C.A., 2003. Net changes in regional woody vegetation cover and carbon storage in Texas drylands, 1937–1999. *Glob. Change Biol.* 9 (3), 316–335.
- Asner, G.P., Elmore, A.J., Olander, L.P., Martin, R.E., Harris, A.T., 2004. Grazing systems, ecosystem responses, and global change. *Annu. Rev. Environ. Resour.* 29, 261–299.
- Barthés, B., Roose, E., 2002. Aggregate stability as an indicator of soil susceptibility to runoff and erosion; validation at several levels. *Catena* 47 (2), 133–149.
- Booth, D.T., Tueller, P.T., 2003. Rangeland monitoring using remote sensing. *Arid Land Res. Manage.* 17 (4), 455–467.
- Breckenfeld, D.J., Svetlik, W.A., McGuire, C.E., 1995. Soil survey of walnut gulch experimental watershed. USDA. Soil Conservation Service Special Report.
- Breshears, D.D., Cobb, N.S., Rich, P.M., Price, K.P., Allen, C.D., Balice, R.G., Meyer, C.W., 2005. Regional vegetation die-off in response to global-change-type drought. *PNAS* 102 (42), 15144–15148.
- Bryant, R., Moran, M.S., McElroy, S.A., Holifield, C., Thome, K.J., Miura, T., Biggar, S.F., 2003. Data continuity of Earth Observing 1 (EO-1) Advanced L and I satellite imager (ALI) and Landsat TM and ETM+. *IEEE Trans. Geosci. Remote Sens.* 41 (6), 1204–1214.
- Burgy, R.H., Pomeroy, C.R., 1958. Interception losses in grassy vegetation. *Eos, Trans. Am. Geophys. Union* 39 (6), 1095–1100.
- Cadaret, E.M., McGwire, K.C., Nouwakpo, S.K., Wetz, M.A., Saito, L., 2016. Vegetation canopy cover effects on sediment erosion processes in the Upper Colorado River Basin Mancos Shale formation, Price, Utah, USA. *Catena* 147, 334–344.
- Cantón, Y., Solé-Benet, A., Asensio, C., Chamizo, S., Puigdefábregas, J., 2009. Aggregate stability in range sandy loam soils relationships with runoff and erosion. *Catena* 77 (3), 192–199.
- Cerdà, A., 1997. The effect of patchy distribution of *Stipa tenacissima* L. on runoff and erosion. *J. Arid Environ.* 36 (1), 37–51.
- Congalton, R.G., 1991. A review of assessing the accuracy of classifications of remotely sensed data. *Remote Sens. Environ.* 37 (1), 35–46.
- Dadkhah, M., Gifford, G.F., 1980. Influence of vegetation, rock cover, and trampling on infiltration rates and sediment production. *J. Am. Water Resour. Assoc.* 16 (6), 979–986.
- DiTomaso, J.M., 2000. Invasive weeds in rangelands: species, impacts, and management. *Weed Sci.* 48, 255–265.
- Dunne, T., Zhang, W., Aubry, B.F., 1991. Effects of rainfall, vegetation, and micro-topography on infiltration and runoff. *Water Resour. Res.* 27 (9), 2271–2285.
- Ebel, B.A., Martin, D.A., 2017. Meta-analysis of field-saturated hydraulic conductivity recovery following wildland fire: applications for hydrologic model parameterization and resilience assessment. *Hydrol. Process.* 31 (21), 3682–3696.
- Emmerich, W.E., 2003. Carbon dioxide fluxes in a semiarid environment with high carbonate soils. *Agric. For. Meteorol.* 116 (1), 91–102.
- Fassnacht, Fabian Ewald, Li, Li, Fritz, Andreas, 2015. Mapping degraded grassland on the Eastern Tibetan Plateau with multi-temporal Landsat 8 data – where do the severely degraded areas occur? *Int. J. Appl. Earth Obs. Geoinf.* 42, 115–127.
- Flerchinger, G.N., Seyfried, M.S., Hardegree, S.P., 2016. Hydrologic response and recovery to prescribed fire and vegetation removal in a small rangeland catchment. *Ecohydrology* 9 (8), 1604–1619.
- Flood, N., 2014. Continuity of reflectance data between landsat-7 ETM+ and landsat-8 OLI, for both top-of-atmosphere and surface reflectance: a study in the Australian landscape. *Remote Sens.* 6 (9), 7952–7970.
- Goodrich, D.C., Schmugge, T.J., Jackson, T.J., Unkrich, C.L., Keefer, T.O., Parry, R., Amer, S.A., 1994. Runoff simulation sensitivity to remotely sensed initial soil water content. *Water Resour. Res.* 30 (5), 1393–1405.
- Goodrich, D.C., Keefer, T.O., Unkrich, C.L., Nichols, M.H., Osborn, H.B., Stone, J.J., Smith, J.R., 2008. Long-term precipitation database, Walnut Gulch Experimental Watershed, Arizona United States. *Water Resour. Res.* 44 (5).
- Goodrich, D.C., Burns, I.S., Unkrich, C.L., Semmens, D.J., Guertin, D.P., Hernandez, M., Levick, L.R., 2012. KINEROS2/AGWA: model use, calibration, and validation. *Trans. ASABE* 55 (4), 1561–1574.
- Greene, R.S.B., Kinnell, P.I.A., Wood, J.T., 1994. Role of plant cover and stock trampling on runoff and soil-erosion from semi-arid wooded rangelands. *Soil Res.* 32 (5), 953–973.
- Guo, X., Wilmschurst, J., McCanny, S., Fargey, P., Richard, P., 2015. Measuring spatial and vertical heterogeneity of grasslands using remote sensing techniques. *J. Environ. Inform.* 3 (1), 24–32.
- Gupta, H.V., Sorooshian, S., Yapo, P.O., 1999. Status of automatic calibration for hydrologic models: comparison with multilevel expert calibration. *J. Hydrol. Eng.* 4 (2), 135–143.
- Gutierrez, J., Hernandez, I.I., 1996. Runoff and interrill erosion as affected by grass cover in a semi-arid rangeland of northern Mexico. *J. Arid Environ.* 34 (3), 287–295.
- Hagen, S.C., Heilman, P., Marssett, R., Torbick, N., Salas, W., Van Ravensway, J., Qi, J., 2012. Mapping total vegetation cover across western rangelands with moderate-resolution imaging spectroradiometer data. *Rangeland Ecol. Manage.* 65 (5), 456–467.
- Havstad, K.M., Peters, D.P., Skaggs, R., Brown, J., Bestelmeyer, B., Fredrickson, E., Wright, J., 2007. Ecological services to and from rangelands of the United States. *Ecol. Econ.* 64 (2), 261–268.
- Hernandez, M., Miller, S. N., Goodrich, D. C., Goff, B. F., Kepner, W. G., Edmonds, C. M., & Jones, K. B. (2000). Modeling runoff response to land cover and rainfall spatial variability in semi-arid watersheds. In *Monitoring Ecological Condition in the Western United States* (pp. 285–298).
- Hernandez, M., Nearing, M.A., Stone, J.J., Pierson, F.B., Wei, H., Spaeth, K.E., Goodrich, D.C., 2013. Application of a rangeland soil erosion model using National Resources Inventory data in southeastern Arizona. *J. Soil Water Conserv.* 68 (6), 512–525.
- Hernandez, M., Nearing, M.A., Al-Hamdan, O.Z., Pierson, F.B., Armendariz, G., Wetz, M.A., Spaeth, K.E., Williams, C.J., Nouwakpo, S.K., Goodrich, D.C., Unkrich, C.L., 2017. The rangeland hydrology and erosion model: a dynamic approach for predicting soil loss on rangelands. *Water Resour. Res.* 53 (11), 9368–9391.
- Herrick, J.E., Van Zee, J.W., Havstad, K.M., Burkett, L.M., Whitford, W.G., 2005. Monitoring manual for grassland, shrubland and savanna ecosystems. Volume I: Quick Start. Volume II: Design, supplementary methods and interpretation. USDA-ARS Jornada Exp. Range.
- Holifield Collins, C.D., Stone, J.J., Cratic, L., 2015. Runoff and sediment yield relationships with soil aggregate stability for a state-and-transition model in southeastern Arizona. *J. Arid Environ.* 117, 96–103.
- Homer, C.G., Dewitz, J.A., Yang, L., Jin, S., Danielson, P., Xian, G., Megown, K., 2015. Completion of the 2011 National Land Cover Database for the conterminous United States-Representing a decade of land cover change information. *Photogramm. Eng. Remote Sens.* 81 (5), 345–354.
- Huete, A.R., 1988. A soil-adjusted vegetation index (SAVI). *Remote Sens. Environ.* 25 (3), 295–309.
- Hunt Jr, E.R., Everitt, J.H., Ritchie, J.C., Moran, M.S., Booth, D.T., Anderson, G.L., Seyfried, M.S., 2003. Applications and research using remote sensing for rangeland management. *Photogramm. Eng. Remote Sens.* 69 (6), 675–693.
- Keefer, T.O., Moran, M.S., Paige, G.B., 2008. Long-term meteorological and soil hydrology database, Walnut Gulch Experimental Watershed, Arizona United States. *Water Resour. Res.* 44 (5).
- Ludwig, J.A., Wilcox, B.P., Breshears, D.D., Tongway, D.J., Imeson, A.C., 2005. Vegetation patches and runoff-erosion as interacting ecophysiological processes in semiarid landscapes. *Ecology* 86 (2), 288–297.
- Markham, B.L., Helder, D.L., 2012. Forty-year calibrated record of earth-reflected radiance from Landsat: a review. *Remote Sens. Environ.* 122, 30–40.
- Marssett, R.C., Qi, J., Heilman, P., Biedenbender, S.H., Watson, M.C., Amer, S., Marssett, R., 2006. Remote sensing for grassland management in the arid southwest. *Rangeland Ecol. Manage.* 59 (5), 530–540.
- Masek, J.G., Vermote, E.F., Saleous, N.E., Wolfe, R., Hall, F.G., Huemmrich, K.F., Lim, T.K., 2006. A Landsat surface reflectance dataset for North America, 1990–2000. *IEEE Geosci. Remote Sens. Lett.* 3 (1), 68–72.
- Mclvor, J.G., Williams, J., Gardener, C.J., 1995. Pasture management influences runoff and soil movement in the semi-arid tropics. *Animal Prod. Sci.* 35 (1), 55–65.
- MEA (Millennium Ecosystem Assessment) *Ecosystems and human well-being*. Vol. 5. Washington, DC: Island Press, 2005.
- Miller, S.N., Kepner, W.G., Mehaffey, M.H., Hernandez, M., Miller, R.C., Goodrich, D.C., Miller, W.P., 2002. Integrating landscape assessment and hydrologic modeling for land cover change analysis. *J. Am. Water Resour. Assoc.*

- Miller, S.N., Semmens, D.J., Goodrich, D.C., Hernandez, M., Miller, R.C., Kepner, W.G., Guertin, D.P., 2007. The automated geospatial watershed assessment tool. *Environ. Modell. Software* 22 (3), 365–377.
- Moran, M.S., Ponce-Campos, G.E., Huete, A., McClaran, M.P., Zhang, Y., Hamerlynck, E.P., Hernandez, M., 2014. Functional response of US grasslands to the early 21st-century drought. *Ecology* 95 (8), 2121–2133.
- Moriassi, D.N., Arnold, J.G., Van Liew, M.W., Bingner, R.L., Harmel, R.D., Veith, T.L., 2007. Model evaluation guidelines for systematic quantification of accuracy in watershed simulations. *Trans. ASABE* 50 (3), 885–900.
- Nearing, M.A., Foster, G.R., Lane, L.J., Finkner, S.C., 1989. A process-based soil erosion model for USDA-Water Erosion Prediction Project technology. *Trans. ASAE* 32 (5), 1587–1593.
- Nearing, M.A., Kimoto, A., Nichols, M.H., Ritchie, J.C., 2005. Spatial patterns of soil erosion and deposition in two small, semiarid watersheds. *J. Geophys. Res. Earth Surf.* 2003–2012, 110(F4).
- Nearing, M., Wei, H., Stone, J., Pierson, F., Spaeth, K., Wetz, M., Flanagan, D., Hernandez, M., 2011. A rangeland hydrology and erosion model. *Trans. ASABE* 54 (3), 901–908.
- Newman, B.D., Wilcox, B.P., Archer, S.R., Breshears, D.D., Dahm, C.N., Duffy, C.J., Vivoni, E.R., 2006. Ecohydrology of water-limited environments: a scientific vision. *Water Resour. Res.* 42 (6).
- Nichols, M.H., Stone, J.J., Nearing, M.A., 2008. Sediment database, Walnut Gulch Experimental Watershed, Arizona United States. *Water Resour. Res.* 44 (5).
- Niraula, R., Norman, L.M., Meixner, T., Callegary, J.B., 2012. Multi-gauge calibration for modeling the semi-arid Santa Cruz Watershed in Arizona-Mexico border area using SWAT. *Air, Soil and Water Res.* 5, 41.
- Norman, L.M., Huth, H., Levick, L., Shea Burns, I., Phillip Guertin, D., Lara-Valencia, F., Semmens, D., 2010. Flood hazard awareness and hydrologic modelling at Ambos Nogales, United States-Mexico border. *J. Flood Risk Manage.* 3 (2), 151–165.
- Nouwakpo, S.K., Wetz, M., Hernandez, M., Champa, T., Fisher, J., 2016a. Performance of the Rangeland Hydrology and Erosion Model for runoff and erosion assessment on a semiarid reclaimed construction site. *J. Soil Water Conserv.* 71 (3), 220–236.
- Nouwakpo, S.K., Williams, C.J., Al-Hamdan, O.Z., Wetz, M.A., Pierson, F., Nearing, M., 2016b. A review of concentrated flow erosion processes on rangelands: fundamental understanding and knowledge gaps. *Int. Soil Water Conserv. Res.* 4 (2), 75–86.
- Pan, C., Shanguan, Z., 2006. Runoff hydraulic characteristics and sediment generation in sloped grassplots under simulated rainfall conditions. *J. Hydrol.* 331 (1), 178–185.
- Park, J.Y., Ale, S., Teague, W.R., Jeong, J., 2017. Evaluating the ranch and watershed scale impacts of using traditional and adaptive multi-paddock grazing on runoff, sediment and nutrient losses in North Texas, USA. *Agric. Ecosyst. Environ.* 240, 32–44.
- Pilgrim, D.H., Chapman, T.G., Doran, D.G., 1988. Problems of rainfall-runoff modelling in arid and semiarid regions. *Hydrol. Sci. J.* 33 (4), 379–400.
- Polyakov, V.O., Nearing, M.A., Stone, J.J., Hamerlynck, E.P., Nichols, M.H., Holifield Collins, C.D., Scott, R.L., 2010. Runoff and erosional responses to a drought-induced shift in a desert grassland community composition. *J. Geophys. Res. Biogeosci.* 2005–2012 115 (G4).
- Puigdefàbregas, J., 2005. The role of vegetation patterns in structuring runoff and sediment fluxes in drylands. *Earth Surf. Proc. Land.* 30 (2), 133–147.
- Purevdorj, T.S., Tateishi, R., Ishiyama, T., Honda, Y., 1998. Relationships between percent vegetation cover and vegetation indices. *Int. J. Remote Sens.* 19 (18), 3519–3535.
- Qi, J., Marsett, R., Heilman, P., Bieden-bender, S., Moran, S., Goodrich, D., Wetz, M., 2002. RANGES improves satellite-based information and land cover assessments in southwest United States. *Eos, Trans. Am. Geophys. Union* 83 (51), 601–606.
- Rawls, W.J., Brakensiek, D.L., Saxton, K.E., 1982. Estimation of soil water properties. *Trans. ASAE* 25 (5), 1316–1320.
- Rawls, W.J., Gimenez, D., Grossman, R., 1998. Use of soil texture, bulk density, and slope of the water retention curve to predict saturated hydraulic conductivity. *Trans. ASAE* 41 (4), 983.
- Reynolds, J.E., Halldin, S., Xu, C.Y., Seibert, J., Kauffeldt, A., 2017. Sub-daily runoff predictions using parameters calibrated on the basis of data with a daily temporal resolution. *J. Hydrol.* 550, 399–411.
- Reynolds, J.F., Smith, D.M.S., Lambin, E.F., Turner, B.L., Mortimore, M., Batterbury, S.P., Walker, B., 2007. Global desertification: building a science for dryland development. *Science* 316 (5826), 847–851.
- Rogers, R.D., Schumm, S.A., 1991. The effect of sparse vegetative cover on erosion and sediment yield. *J. Hydrol.* 123 (1), 19–24.
- Ross, M., 2013. Using the rangeland hydrology and erosion model to assess rangeland management practices on the Kaler ranch. (Unpublished master's thesis). University of Arizona, United States.
- Roy, D.P., Wulder, M.A., Loveland, T.R., Woodcock, C.E., Allen, R.G., Anderson, M.C., Scambos, T.A., 2014. Landsat-8: science and product vision for terrestrial global change research. *Remote Sens. Environ.* 145, 154–172.
- Schlesinger, W.H., Reynolds, J.F., Cunningham, G.L., Huenneke, L.F., Jarrell, W.M., Virginia, R.A., Whitford, W.G., 1990. Biological feedbacks in global desertification. *Science* 247 (4946), 1043–1048.
- Scholes, R.J., Archer, S.R., 1997. Tree-grass interactions in savannas. *Annu. Rev. Ecol. Syst.* 517–544.
- Scott, R.L., Hamerlynck, E.P., Jenerette, G.D., Moran, M.S., Barron-Gafford, G.A., 2010. Carbon dioxide exchange in a semidesert grassland through drought-induced vegetation change. *J. Geophys. Res. Biogeosci.* 115 (G3).
- Seyfried, M.S., Wilcox, B.P., 1995. Scale and the nature of spatial variability: field examples having implications for hydrologic modeling. *Water Resour. Res.* 31 (1), 173–184.
- Sibanda, M., Mutanga, O., Rouget, M., 2016. Discriminating rangeland management practices using simulated hyperspectral, Landsat 8 OLI, Sentinel 2 MSI, and VENUS spectral data. *IEEE J. Sel. Top. Appl. Earth Obs. Remote Sens.* 9 (9), 3957–3969.
- Smith, R.E., Parlange, J.Y., 1978. A parameter-efficient hydrologic infiltration model. *Water Resour. Res.* 14 (3), 533–538.
- Smith, R.E., Goodrich, D.C., Woolhiser, D.A., Unkrich, C.L., 1995. KINEROS—a kinematic runoff and erosion model. *Computer Models Watershed Hydrol.* 20, 627–668.
- Spaeth, K.E., Wetz, M.A., Williams, C.J., Pierson, F.B., 2016. Plant/Life Form Considerations in the Rangeland Hydrology and Erosion Model (RHEM). 10th International Rangeland Congress, pp. 1048.
- Stehman, S.V., Czaplewski, R.L., 1998. Design and analysis for thematic map accuracy assessment: fundamental principles. *Remote Sens. Environ.* 64 (3), 331–344.
- Stone, J.J., Nichols, M.H., Goodrich, D.C., Buono, J., 2008a. Long-term runoff database, Walnut Gulch Experimental Watershed, Arizona United States. *Water Resour. Res.* 44 (5).
- Tarantino, C., Adamo, M., Lucas, R., Blonda, P., 2016. Detection of changes in semi-natural grasslands by cross correlation analysis with WorldView-2 images and new Landsat 8 data. *Remote Sens. Environ.* 175, 65–72.
- Thurow, T.L., Blackburn, W.H., Warren, S.D., Taylor Jr, C.A., 1987. Rainfall interception by midgrass, shortgrass, and live oak mottes. *J. Range Manag.* 455–460.
- Tucker, C.J., 1979. Red and photographic infrared linear combinations for monitoring vegetation. *Remote Sens. Environ.* 8 (2), 127–150.
- Urban, D.L., 2005. Modeling ecological processes across scales. *Ecology* 86 (8), 1996–2006.
- Vicente-Serrano, S.M., Beguería, S., López-Moreno, J.I., Angulo, M., El Kenawy, A., 2010. A new global 0.5 gridded dataset (1901–2006) of a multiscalar drought index: comparison with current drought index datasets based on the Palmer Drought Severity Index. *J. Hydrometeorol.* 11 (4), 1033–1043.
- Villarreal, M.L., Norman, L.M., Buckley, S., Wallace, C.S., Coe, M.A., 2016. Multi-index time series monitoring of drought and fire effects on desert grasslands. *Remote Sens. Environ.* 183, 186–197.
- Vermote, E., Justice, C., Claverie, M., Franch, B., 2016. Preliminary analysis of the performance of the Landsat 8/OLI land surface reflectance product. *Remote Sens. Environ.*
- Vogelmann, J.E., Xian, G., Homer, C., Tolk, B., 2012. Monitoring gradual ecosystem change using Landsat time series analyses: case studies in selected forest and rangeland ecosystems. *Remote Sens. Environ.* 122, 92–105.
- Wainwright, J., Parsons, A.J., Abrahams, A.D., 2000. Plot-scale studies of vegetation, overland flow and erosion interactions: Case studies from Arizona and New Mexico. *Hydrol. Process.* 14 (16–17), 2921–2943.
- Wallace, J., Behn, G., Furby, S., 2006. Vegetation condition assessment and monitoring from sequences of satellite imagery. *Ecol. Manage. Restor.* 7 (s1), S31–S36.
- Wetz, M.A., Arslan, Awadis B., Lane, Leonard J., 1992. Hydraulic roughness coefficients for native rangelands. *J. Irrig. Drain. Eng.* 118 (5), 776–790.
- Williams, C.J., Pierson, F.B., Spaeth, K.E., Brown, J.R., Al-Hamdan, O.Z., Wetz, M.A., Nearing, M.A., Herrick, J.E., Boll, J., Robichaud, P.R., Goodrich, D.C., 2016a. Application of ecological site information to transformative changes on Great Basin sagebrush rangelands. *Rangelands* 38 (6), 379–388.
- Williams, C.J., Pierson, F.B., Robichaud, P.R., Al-Hamdan, O.Z., Boll, J., Strand, E.K., 2016b. Structural and functional connectivity as a driver of hillslope erosion following disturbance. *Int. J. Wildland Fire* 25 (3), 306–321.
- Wulder, M.A., Masek, J.G., Cohen, W.B., Loveland, T.R., Woodcock, C.E., 2012. Opening the archive: How free data has enabled the science and monitoring promise of Landsat. *Remote Sens. Environ.* 122, 2–10.
- Xie, Y., Sha, Z., Yu, M., 2008. Remote sensing imagery in vegetation mapping: a review. *J. Plant Ecol.* 1 (1), 9–23.
- Xu, D., Koper, N., Guo, X., 2018. Quantifying the influences of grazing, climate and their interactions on grasslands using Landsat TM images. *Grassland Sci.* 64 (2), 118–127.
- Zuazo, V.D., Pleguezuelo, C.R., Martínez, J.F., Rodríguez, B.C., Raya, A.M., Galindo, P.P., 2008. Harvest intensity of aromatic shrubs vs. soil erosion: an equilibrium for sustainable agriculture (SE Spain). *Catena* 73 (1), 107–116.